Journal of Materials Chemistry C

ROYAL SOCIETY OF CHEMISTRY

PAPER

View Article Online
View Journal | View Issue

Cite this: J. Mater. Chem. C, 2025, 13, 14518

Stretchable light-emitting electrochemical cells fabricated by spray-coating†

Sandra Gellner,*[ab] Etienne Auroux,[b] Joan Ràfols-Ribé,[bc] Nicole Stracke,[d] Kumar Saumya,[b] Anton Kirch,[b] Christian Larsen,[bc] Ekaterina Nannen[a] and Ludvig Edman*[bce]

Received 3rd December 2024,
Accepted 7th June 2025

DOI: 10.1039/d4tc05108d

rsc.li/materials-c

Intrinsically stretchable emissive devices that are thin, lightweight and low-cost are highly desired for, *e.g.*, wearable electronics, where they can enable facile communication and interaction with, and adaptability to, dynamic environments. The light-emitting electrochemical cell (LEC) is a candidate for the fulfillment of these challenging requirements, since its robust and air-stabile device architecture renders it a good fit for cost-efficient, ambient-air printing and coating fabrication of intrinsically stretchable thin-film device architectures. Here, we report on the design and pioneering fabrication of such an intrinsically stretchable LEC by non-interrupted spray-coating under ambient air and show that such an optimized, and potentially low-cost, thin-film LEC can deliver uniform light emission from a lightweight device architecture even at 30% lateral elongation.

Introduction

Stretchable and flexible devices are essential components in wearable electronics, with demonstrated or projected applications in a vast and intriguing range of fields, including healthcare, protective gear, sports, and fashion.[1–8] Stretchability was initially inferred by advanced engineering of rigid devices, in the form of buckled device designs,[9–13] the introduction of stretchable interconnections,[14–18] or origami and kirigami folding and cutting.[19–22] However, there is currently a shift in focus towards *intrinsically* stretchable devices, as motivated by their much higher mechanical robustness compared to devices that achieve stretchability through structural design.[23] Notably, displays and actuators for the visualization of data and communication of information are increasingly required to be intrinsically stretchable in order to meet the stringent requirements of advanced and projected future applications.[24–27]

The organic light-emitting diode (OLED) can deliver high-efficiency emission from thin-film and lightweight device architectures, and they can also be fabricated as intrinsically stretchable devices.[26,28–31] However, since OLEDs commonly comprise a multitude of very thin (few nm thick) layers stacked on top of each other, and since all the different layers in an intrinsic stretchable device need to be stretchable and robust, this development towards intrinsic stretchability in OLEDs has proven challenging. Moreover, for the same reason it is very difficult to fabricate complete OLEDs with cost-efficient and scalable printing and coating methods.

In this context, the lightweight and thin-film light-emitting electrochemical cell (LEC) technology emerges as an interesting alternative, in part because of its more robust and air-stabile three-layer device architecture.[32–37] More specifically, the LEC commonly comprises an emissive active material sandwiched between two air-stable electrodes, at least one of which is transparent. The active material consists of an electroluminescent organic semiconductor blended with mobile ions. When a voltage is applied between the two electrodes, the mobile ions start to drift to first form electric double layers at the electrode interfaces, which facilitate for the efficient and balanced injection of holes and electrons. The first injected holes and electrons attract compensating counterions for the formation of electrochemical p- and n-doping regions near the electrodes, which grow together for the formation of a p–n junction.[38] Here, subsequently injected holes and electrons form excitons, which can decay radiatively. This unique LEC operational mechanism enables the employment of a rather thick (compared to the OLED) single-layer active material, air-stabile electrodes and relatively rough substrates,[39] which in turn has paved the way for the fabrication of complete LECs by

[a] Competence Centre for Novel Electronics and Advanced Materials, Faculty of Engineering and Computer Science, University of Applied Sciences Niederrhein, 47805, Krefeld, Germany
[b] The Organic Photonics and Electronics Group, Department of Physics, Umeå University, SE-90187, Umeå, Sweden. E-mail: ludvig.edman@umu.se
[c] LunaLEC AB, Umeå University, SE-90187, Umeå, Sweden
[d] Werkstoffe der Elektrotechnik and CENIDE, University of Duisburg-Essen, 47057, Duisburg, Germany
[e] Wallenberg Initiative Materials Science for Sustainability, Department of Physics, Umeå University, SE-90187, Umeå, Sweden

† Electronic supplementary information (ESI) available. See DOI: https://doi.org/10.1039/d4tc05108d

ambient-air printing and coating methods.[40–45] These characteristics, in combination with earlier demonstrations of flexible LEC devices,[43,46] suggest that the LEC technology also could be well-suited for a scalable printing and coating fabrication of intrinsically stretchable emissive devices.

The first stretchable LEC was reported by Yu *et al.* in 2011, and it comprised two laminated electrodes; however, a drawback from a scalability and cost perspective was that the active material was deposited by non-scalable and material-inefficient spin-coating.[47] One year later, Filiatrault and co-workers reported a stretchable LEC, which featured a spin-coated active material positioned between a vacuum-deposited Au anode and a drop-cast eutectic gallium–indium cathode.[48] In 2013, Liang *et al.* developed a stretchable LEC, which comprised a spin-coated active material sandwiched between a spin-coated poly(3,4-ethylenedioxythiophene):poly(styrene sulfonate) (PEDOT:PSS) anode and a laminated silver nanowire (AgNW) cathode, which delivered a luminance of 30 cd m^{-2} at 120% elongation.[49] Liu and co-workers reported on the integration of a stretchable LEC (fabricated with a similar procedure as Liang *et al.*)[49] with stretchable thin-film transistors, which demonstrated that LECs can function as the emissive component in a stretchable active-matrix display.[25] Finally, Han *et al.* recently reported an intrinsically stretchable LEC, which delivered an impressive emission performance, but which comprised a spin-coated active material sandwiched between a spin-coated PEDOT:PSS:non-ionic-surfactant anode and a laminated AgNW:graphene cathode.[50] Table S1 in the ESI† provides a summary of some key fabrication and performance metrics of early reported stretchable LECs.

Thus, despite these promising achievements, the demonstration of a stretchable LEC that is solely fabricated by scalable printing and coating methods, and therefore practically relevant, is lacking. Herein, we report on the ambient-air spray-coating fabrication of a complete LEC device, which delivers uniform light emission even when stretched to an elongation of 30%. This demonstration is notable in the context of that ambient-air spray-coating can be scalable and low cost, and since the developed LEC in addition to being stretchable also is thin and lightweight. The intrinsically stretchable LEC consisted of a PEDOT:PSS/AgNW bilayer cathode and a transparent PEDOT:PSS anode, which sandwiched an active material, comprising a high-molecular-weight conjugated polymer, a hydrophobic ionic liquid and a polymeric poly(urethane) (PU) mechanical stabilizer. It was specifically demonstrated that the AgNW layer should contact the active material in order to inhibit side reactions, whereas the inclusion of PU improved the mechanical properties and the robustness of the device.

Experimental

Materials

The stretchable 21 × 30 cm^2 substrates (Beyolex, Panasonic) were cut into 1.5 × 4 cm^2 rectangles, but otherwise used as received. A specific poly(3,4-ethylenedioxythiophene)-poly(styrenesulfonate) (PEDOT:PSS) dispersion (catalogue number: SV3, Heraeus, GER) was selected based on its previous good performance in LEC devices.[44] This PEDOT:PSS dispersion was diluted with 400 vol% of methanol, followed by 45 min sonication in an ultrasonic bath (VWR, GER), for the formulation of a PEDOT:PSS ink with appropriate viscosity for spray deposition. Two different silver nanowire (AgNW) dispersions were investigated (10 mg ml^{-1} in ethanol, ∅ 90 nm, length: 20–50 μm, Blue Nano; 5 mg ml^{-1} in isopropyl alcohol, ∅ 60 nm, length: 10 μm, Sigma Aldrich) with similar results. The selected AgNW dispersion was diluted with 1900 vol% of isopropanol and sonicated for 20 min in an ultrasonic bath for the formulation of the AgNW ink. Poly(methyl methacrylate) (PMMA, Sigma-Aldrich, GER) was dissolved in butyl acetate in a concentration of 20 mg ml^{-1} and stirred at 70 °C for >24 h in a N_2-filled glovebox ($[O_2] < 1$ ppm, $[H_2O] < 1$ ppm). This solution was diluted with 450 vol% ethyl acetate under ambient air for the formulation of the PMMA ink.

The constituents of the active material were the electroluminescent organic semiconductor Super Yellow (SY, catalogue number: PDY-132, Merck, GER), the ionic liquid tetrahexylammonium tetrafluoroborate ($THABF_4$, Merck, GER), and, in some cases a polyurethane thermoplastic (PU, Estane® 58887, Good-Fellow, UK). The constituents were separately dissolved in cyclohexanone in a concentration of 10 mg ml^{-1} and thereafter stirred at 70 °C for >24 h in the N_2-filled glovebox. The active-material constituents were mixed in two (SY : $THABF_4$: PU) mass ratios: (1 : 0.15 : 0) or (1 : 0.15 : 0.49). Cyclohexanone was thereafter added to render the total solute concentration (*i.e.* the total mass of the active-material components divided by the total volume of cyclohexanone) 8 mg ml^{-1}. These blend solutions were stirred at 70 °C for >24 h, whereafter they were further diluted by 450 vol% tetrahydrofuran (THF, Merck, GER) under ambient air for the formulation of the two active-material inks.

Electrode and device fabrication

The stretchable LECs, including both stretchable electrodes, were deposited by ambient-air spray-coating, using a computer-controlled spray box (LunaLEC, SWE) equipped with an internal-mix spray nozzle (Techcon system, US). The sample to be spray-coated was put on a hot plate, which was kept at 80 °C during the spray-coating deposition. The shadow masks were fabricated by 3D printing of polyethylene terephthalate modified with glycol (PolyLite PETG Black, Polymaker).

The PEDOT:PSS ink was spray-coated onto the stretchable substrate through a shadow mask that defined a PEDOT:PSS area of 0.3 × 2.2 cm^2, as illustrated in Fig. 1(a). The parameters for the spray-coating of the PEDOT:PSS ink were: N_2 gas pressure = 410 kPa, ink flow rate = 4 ml min^{-1}, number of sweeps = 3, spray time = 60 s. The spray-coated PEDOT:PSS layer was dried in a vacuum oven at 120 °C for 4 min. The AgNW ink was spray-coated through the same shadow mask, using the following parameters: N_2 gas pressure = 345 kPa, ink flow rate = 2.5 ml min^{-1}, number of sweeps = 13, spray time = 260 s. The fabrication of the PEDOT:PSS/AgNW bilayer cathode is schematically depicted in Fig. 1(a). The PMMA ink was spray-coated through a shadow mask, which is the inverse of the cathode shadow mask, using the following parameters: N_2 gas pressure = 450 kPa, ink flow rate = 4 ml min^{-1},

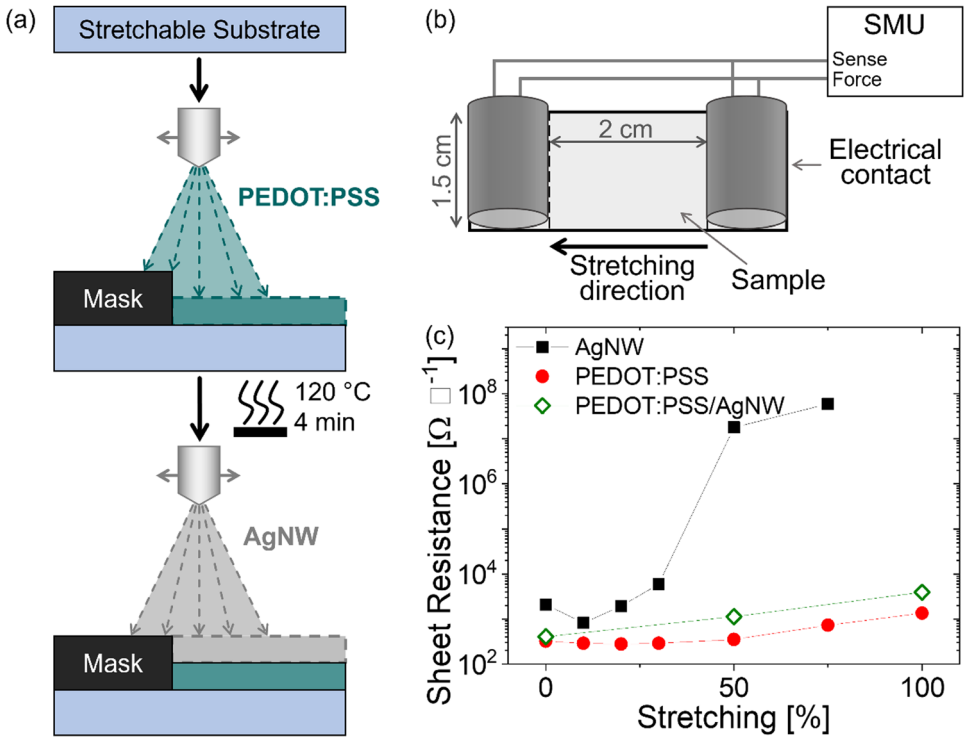

Fig. 1 (a) Schematic presentation of the key steps in the sequential spray-coating fabrication of the PEDOT:PSS/AgNW bilayer electrode on top of the stretchable substrate. (b) Schematic showing the resistance measurement of the electrodes during stretching. (c) The evolution of the *in situ* measured sheet resistance during lateral stretching of the following three 2 × 1.5 cm^2 planar electrodes: single-layer AgNW (solid black squares), single-layer PEDOT:PSS (solid red circles), and bilayer PEDOT:PSS/AgNW (open green diamonds). All three electrodes were fabricated on the stretchable substrate using the spray-coating procedure depicted in (a).

number of sweeps = 4, spray time = 80 s. The role of the insulating PMMA layer is to suppress the risk for short circuits and to accurately define the emission area.

The active-material ink was spray-sintered on top of the bilayer cathode, with the following parameters: N_2 gas pressure = 450 kPa, ink flow rate = 4 ml min^{-1}; the number of sweeps was 8, resulting in a spray time of 160 s. An important advantage of spray-sintering (compared to, *e.g.*, spray-coating) is that phase separation between the different solid constituents in the deposited film is suppressed, as discussed in detail in ref. 51. The PMMA ink was spray-coated on top of the active material through a shadow mask, using the same parameters as specified above. The PEDOT:PSS ink was finally spray-coated through a shadow mask, which was the inverse of the second PMMA shadow mask, using the same parameters as above. The PEDOT:PSS top anode was dried in a vacuum oven at 120 °C for 4 min, and its overlap with the bottom cathode defined the 3 × 4 mm^2 emission area. All of the above deposition steps were performed under ambient air.

The rigid reference LECs were fabricated on pre-patterned indium tin oxide (ITO) coated glass substrates (substrate area = 30 × 30 mm^2, ITO thickness = 145 nm, thin film devices, US), which were cleaned by sequential 15 min ultrasonic sonication in detergent (Extran MA 01, Merck, GER), distilled water, acetone, and isopropanol. The cleaned substrates were dried at 120 °C for ≥ 24 h, whereafter the active-material ink was spray-sintered on top of the ITO with the following parameters: N_2 gas pressure = 450 kPa, ink flow rate = 4 ml min^{-1}, number of sweeps = 5, and spray time = 100 s. In order to study the influence of PU in the active layer, the active-material constituents were mixed in four (SY : $THABF_4$: PU) mass ratios: (1 : 0.15 : 0), (1 : 0.15 : 0.49), (1 : 0.15 : 1.15), and (1 : 0.15 : 2.68). A top Al cathode, with a thickness of 100 nm, was deposited by thermal evaporation (p = 0.3 mbar) through a shadow mask. The overlap between the bottom ITO anodes and the top Al cathodes defined four 2 × 2 mm^2 reference LECs on each glass substrate.

Electrode and device characterization

The elongation of the stretchable electrodes and the stretchable LECs was executed by mounting the device under test on a custom-built stretching apparatus, with the extent of stretching being controlled by a custom-made Python program. The surface topography and the morphology of the spray-coated PEDOT:PSS and AgNW films on the Beyolex substrates following lateral stretching and relaxation were measured with atomic force microscopy (AFM, Park NX-HiVac system) and scanning electron microscopy (SEM, Supra 25, Zeiss AG). The AFM imaging was performed in in non-contact mode at a scan rate of 0.2 Hz, using a silicon cantilever featuring a spring constant of 42 Nm^{-1}. The images were post-processed using the software Gwyddion. For the device characterization, a source-measure unit (SMU, Keithley

2400) applied the voltage and measured the current during stretching, as depicted in Fig. 1(b). The luminance of the stretchable LEC was measured with a SMU-controlled photodiode (V27 BPW21R 148), positioned 2 mm away from the surface of the transparent PEDOT:PSS anode. The photodiode had previously been calibrated with a luminance meter (LS-110, Konica Minolta). The rigid reference LECs were measured in a commercial setup (M6000 PMX, McScience, KOR), with the constant drive voltage being 4 V and the current density compliance being 250 mA cm^{-2}. The characterization of the stretchable electrodes and the stretchable and rigid reference LECs was performed in a N_2-filled glovebox ($[O_2] < 1$ ppm, $[H_2O] < 1$ ppm).

Statistical analysis

For the initial evaluation of electrode stretchability, 11 independent electrode films were fabricated and characterized, and the performance was found to be highly repeatable with, *e.g.*, the standard deviation in the sheet resistance being 10% or smaller. For the stretchable-LEC evaluation, more than 20 independent devices were fabricated and measured. Their distribution and baseline functionality are summarized in Fig. S4 (ESI†), and the presented performance data in Fig. 3 was collected on a representative device within the set of functional devices.

Results and discussion

The development of an intrinsically stretchable LEC device requires that all layers are inherently stretchable, including the active material, both electrodes and the substrate. Here, we elected to employ a commercially available stretchable substrate, which can be stretched to 200% elongation. For the stretchable electrodes, we identified PEDOT:PSS and AgNW as promising candidates, since they exhibit high transparency, high conductivity, and capacity for solution-based processing,[30,52–54] and since they previously have demonstrated function in stretchable (and flexible) devices.[25,40,45,49]

We evaluated the electrode and substrate materials by first spray-coating three different 4×1.5 cm^2 conducting films – single-layer PEDOT:PSS, single-layer AgNW, and bilayer PEDOT:PSS/AgNW – on top of the stretchable substrate, and then measuring their electrical resistivity and stability *in situ* during stretching. Fig. 1(a) depicts schematically the key deposition, masking and drying steps of the sequential spray-coating fabrication of the bilayer PEDOT:PSS/AgNW electrode, as executed with our home-built spray-coating apparatus under ambient air. The single-layer PEDOT:PSS and single-layer AgNW electrodes were fabricated with the same spray-coating procedure and apparatus. The PEDOT:PSS layer was dried at 120 °C in a vacuum oven for 4 min following the spray-coating deposition. A visual inspection of the three electrode-on-substrate assemblies following the final drying step revealed no signs of mechanical damage or warping. Further details on the electrode fabrication can be found in the Experimental section.

Fig. 1(b) depicts the lateral direction of electrode stretching and the four-probe current–voltage test setup, which was employed to determine the *in situ* evolution of the sheet resistance during lateral stretching. Fig. 1(c) shows that the single-layer PEDOT:PSS electrode (solid red circles) and the bilayer PEDOT:PSS/AgNW electrode (open green diamonds) exhibits a similar sheet resistance of $\sim 375\ \Omega\ \square^{-1}$ in the non-stretched state, while the single-layer AgNW electrode (solid black squares) exhibits a notably higher sheet resistance of $2100\ \Omega\ \square^{-1}$ in the non-stretched state. Interestingly, the sheet resistance of the single-layer AgNW electrode is observed to decrease by the first stretching to 10% elongation, but at stretching above 30% elongation it features a rapid but reversible increase of the resistance, and at an elongation above 75% its resistance increases dramatically. The single-layer PEDOT:PSS electrode was much more robust towards stretching, and at an elongation to twice its original lateral length (100% stretching) the sheet resistance had only increased by a factor eight compared to the unstretched sheet resistance without any sign of structural breakdown.

We performed high-resolution imaging of the morphology and the topography of the single-layer AgNW electrode and the single-layer PEDOT:PSS electrode with scanning electron microscopy (SEM, Fig. S1, ESI†) and atomic force microscopy (AFM, Fig. S2, ESI†). Both the morphology and the topography of the AgNW electrode remained essentially invariant following relaxation after a lateral stretching of up to 30%, whereas the PEDOT:PSS electrode in contrast featured strong buckling in both AFM and SEM that increased in magnitude with increasing degree of preceding lateral stretching.

With these observations at hand, we propose that the AgNWs start to separate and lose contact during the lateral stretching (thus the increase of the resistance), but also that this effect is reversible (up to 30% elongation) and that this explains why the morphology and topography of the AgNW film remain invariant after the stretching. In contrast, the PEDOT:PSS film irreversibly buckles during stretching, but the contact between the soft polymer chains remains which explains the relatively small resistance increase.

However, a drawback with PEDOT:PSS is that it has been demonstrated to be a non-ideal cathode material for LECs.[44] More specifically, the electronic conductivity of PEDOT:PSS originates from that the PEDOT polymer is p-type doped (with PSS being the negative counterion), but when biased negative (*i.e.* when functioning as the cathode in a LEC) it can become electrochemically undoped, and thereby rendered poorly conductive.[44] Ag has in contrast been demonstrated to function as a high-performance stabile cathode material in common LECs.[55] This was thus our main motivation for the fabrication of the bilayer PEDOT:PSS/AgNW electrode, where the intention was that the AgNW layer was to be positioned in contact with the LEC active material while the PEDOT:PSS layer was providing for high stretchability. Reassuringly, the bilayer PEDOT:PSS/AgNW electrode performed similarly to the single-layer PEDOT:PSS electrode during stretching, with the sheet resistance only increasing by a factor of twenty when stretched to 100% elongation. The higher stability of the electrical transport capacity of the bilayer PEDOT:PSS/AgNW electrode towards elongation compared to the single-layer AgNW electrode implies that PEDOT:PSS effectively functions as a conductive and stretchable glue in

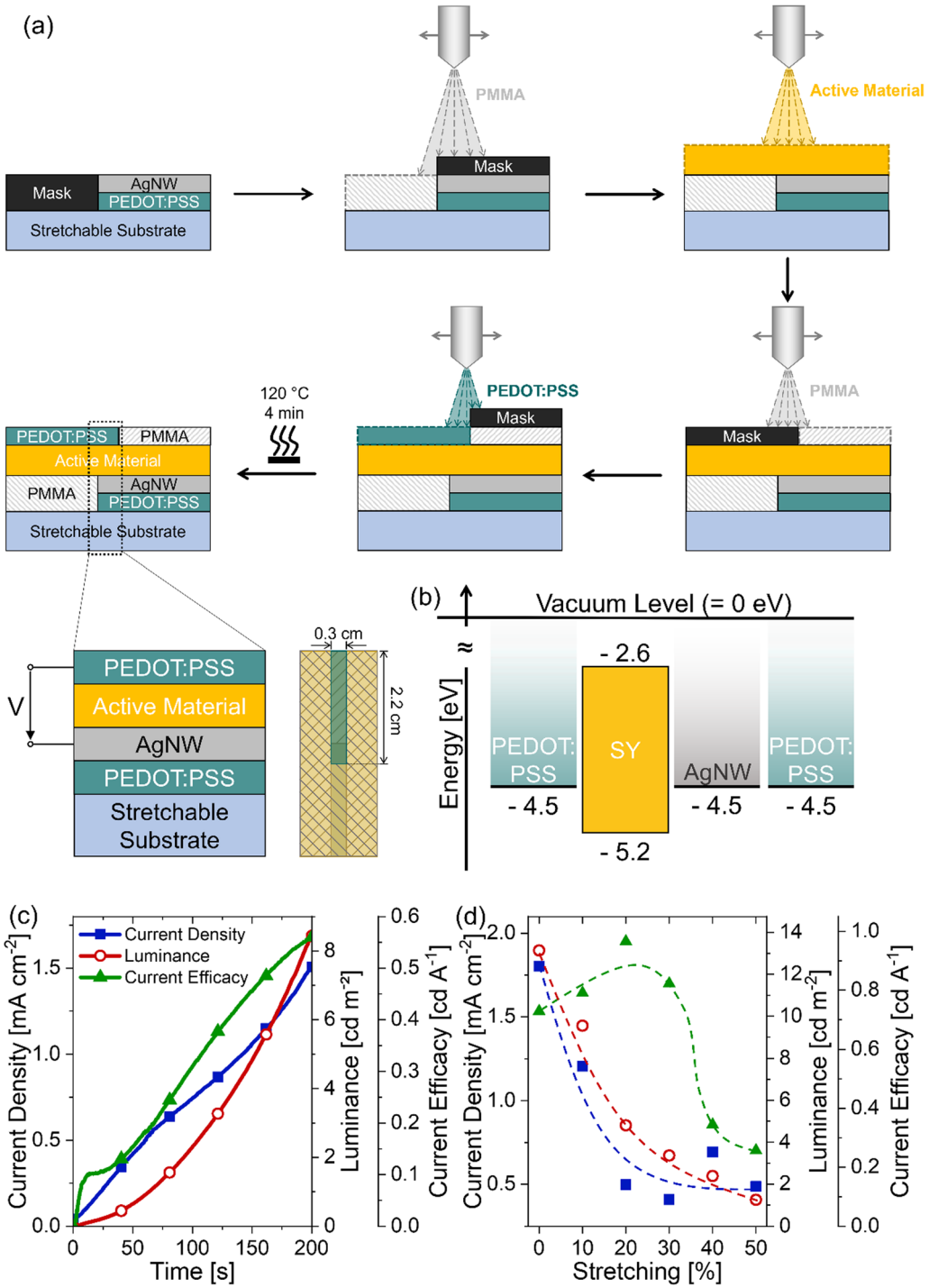

Fig. 2 (a) Schematic showing the final steps of the fabrication of the stretchable LEC, *i.e.* the spray-coating fabrication of the active material, the pattering layers, and the top PEDOT:PSS anode on top of a stretchable-substrate/PEDOT:PSS/AgNW assembly. The panel figure presents a side-view and a top-view presentation of the complete device stack. (b) The electron-energy diagram of the stretchable LEC equipped with a bilayer PEDOT:PSS/AgNW cathode and a PEDOT:PSS anode, with values for the Fermi levels and the frontier orbitals derived from ref. 44 and 56. (c) The initial temporal evolution of the current density (solid blue squares), the luminance (open red circles) and the current efficacy (solid green triangles) of a pristine non-stretched LEC during driving by a constant voltage of 20 V. (d) The measured peak values for the current density, the luminance and the current efficacy of the stretchable LEC as a function of stretching. The dashed lines are a guide to the eye.

between different AgNWs. This suggests that the bilayer PEDOT:PSS/AgNW electrode could be a viable cathode material in a stretchable LEC.

We specifically employed the PEDOT:PSS/AgNW bilayer on top of the stretchable substrate as our bottom cathode. Fig. 2(a) presents the scheme for the subsequent spray deposition of the

poly(methyl methacrylate) (PMMA) patterning layers, the emissive active material, and the top transparent PEDOT:PSS anode, as well as the complete device architecture of the stretchable LEC in cross-sectional side view and in top view. A more detailed presentation of the fabrication process is provided in Fig. S3 (ESI†). The active material comprised the electroluminescent organic semiconductor Super Yellow (SY) and the ionic liquid $THABF_4$ in a 100 : 15 mass ratio. These two active-material constituents were selected since they both are highly hydrophobic and thereby are anticipated to tolerate (*i.e.* remain physically intact after) the subsequent deposition of the hydrophilic PEDOT:PSS ink, and since the SY majority component has been reported to feature high stretchability by the virtue of being an amorphous high-molecular-weight polymer.[49] Directly after the final spray-coating deposition, the complete stretchable LEC was dried at 120 °C for 4 min. We call attention to that the entire device fabrication was performed under ambient air, using additive, material-efficient and scalable spray coating for all deposition steps.

Fig. 2(b) is the electron-energy diagram of the stretchable LEC. We note that the barriers for electron injection (1.9 eV) and hole injection (0.7 eV) are large and highly asymmetric. We do however anticipate that efficient and balanced electron and hole injection will be achieved by an initial migration of the mobile ions in the active material, which will lead to the formation of injection-facilitating electric double layers at the electrode interfaces. We further anticipate that the first injected electrons and holes will be electrically compensated by further ion redistribution, and thereby enable for transport-enhancing electrochemical n- and p-type doping, respectively, of SY.

Fig. 2(c) presents the measured initial temporal evolution of the current density (solid blue squares), the luminance (open red circles), and the current efficacy (solid green triangles) for a pristine stretchable LEC (in the non-stretched state) when driven by a constant voltage of 20 V. The observed transient increase for all three parameters is in line with that injection-facilitating electric double layers are forming at the electrode interfaces and that transport-enhancing electrochemical doping of SY takes place. This LEC-characteristic observation thus provides support for that we have managed to fabricate a functional LEC, and the next task is thus to investigate its performance during stretching.

After 6 min of constant-voltage operation, the LEC was exposed to a lateral stretching step of 10% elongation every 60 s, up to a maximum elongation of 50% (see Fig. 1b, for presentation of the stretching geometry). Fig. 2(d) presents the measured values of the current density, luminance and current efficacy as a function of stretching. At 30% stretching, the current density and luminance have dropped by a factor of three, whereas the current efficacy in contrast remained essentially constant. At further stretching, the current efficacy begins to drop markedly, and at an elongation of the device above 50%, all three parameters irreversibly drop to zero, which implies that irreversible breakdown has taken place. It thus appears as though the first stretching to 30% elongation mainly affects the electrical transport, but that further stretching up to 50% also results in deterioration of the emissive capacity; and that a stretching to 50% elongation in the lateral direction is the limit that this particular device architecture can handle mechanically.

A persistent drawback with this first stretchable LEC configuration was the frequent observation of a very rapid transient increase of the current density (and the luminance) followed by a similarly very rapid drop (see Fig. S4, ESI†). We assign these short-term transient events to the formation of local ''hot spots'' by short circuits. Their presumed origin is that the relatively long ($\geq$10 μm) AgNWs at the cathode surface protrude through the much thinner layer of active material, while their subsequent disappearance is attributed to the concomitant local self-heating caused by the high local current density.

In order to effectively suppress these non-desired short-circuit events and to improve the stretching stability and mechanical robustness of the LEC, a third robust component was added to the active material, in the form of a polyurethane (PU) polymer. PU was selected for this task since it simultaneously features high durability, toughness and chemical resistance[57] (and since it in addition has been reported that PU can be biocompatible and biodegradable).[58] However, an obvious challenge from an electrical transport perspective could be that PU is an electronic insulator, but we do note that its combination with SY in the emissive material of an OLED was reported to result in improved device performance.[30]

The optimum PU load in the active material was determined through a systematic investigation using a rigid-reference LEC, which comprised the same spray-coated active material but vacuum-deposited ITO and Al for the electrodes. Fig. S5 (ESI†) reveals that the addition of PU did, as expected, lower the current density, but also that the specific addition of 30 wt% PU left the luminance relatively non-affected. Combined, this has the interesting consequence that the current efficacy was increased by the addition of 30 wt% PU. The addition of a higher PU load did however lead to a dramatic drop of the luminance, and therefore a 30 wt% load of PU in the active material was used from hereon.

The ''stretchable PU-LEC'' was fabricated with the same procedure outlined in Fig. 2(a), but with 30 wt% PU added to the active-material ink. Importantly, we find that this addition of PU to the active material, as desired, resulted in a significant suppression of the short-circuit problem for the stretchable PU-LEC compared to the PU-free stretchable LEC (see Fig. S4 for details, ESI†). A comparison of the performance of the PU-free and the PU-containing devices during repeated stretching is provided in Fig. 3. The two devices were first pre-biased at 40 V for 60 s in the non-stretched state, and thereafter exposed to five cycles of 60 s/60 s stretching-to-10%-elongation/relaxation and five subsequent 60 s/60 s stretching-to-20%-elongation/relaxation cycles. Fig. S6 (ESI†) presents the complete temporal evolution of this on/off stretching cycling experiment.

The original non-stretched performance after the pre-bias stage was relatively similar, although the PU-LEC exhibited slightly higher values for the current density (Fig. 3a), the luminance (Fig. 3b) and the current efficacy (Fig. 3c). The response to the first stretching to 10% elongation is however markedly different.

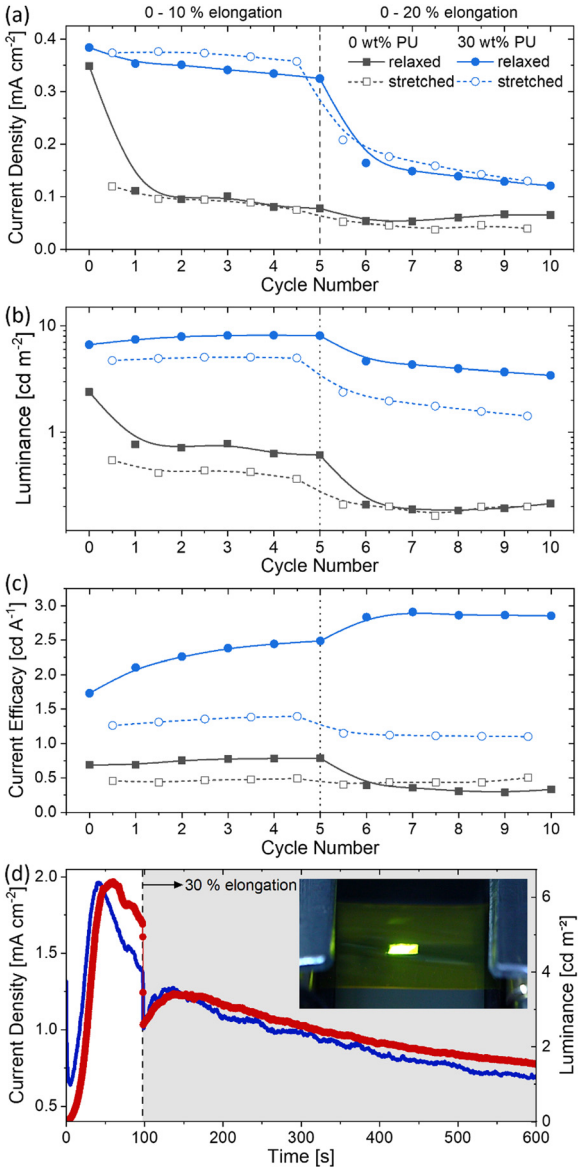

Fig. 3 (a)–(c) The stretching/relaxation performance of the PU-free LEC (grey squares) and the PU-LEC (blue circles) during constant-voltage driving. The devices were first pre-biased at 40 V for 60 s (data not shown), and thereafter first cycled five times between 0 and 10% elongation and thereafter five times between 0 and 20% elongation. Each dwell time in the stretched state and the relaxed state was 60 s. (d) The temporal evolution of the current density (blue line) and the luminance (solid red circles) of the PU-LEC during constant-bias driving by 40 V. The device was stretched to 30% elongation after 100 s of operation. The inset is a photograph of the uniform luminance of the PU-LEC during stretching to 30% elongation.

Whereas the current density and the luminance only are decreasing marginally for the PU-LEC, the drop of both the current and luminance is rather dramatic for the PU-free LEC. In fact, the current density remained more than three times higher and the luminance more than five times higher, in both the relaxed and stretched state, for the PU-LEC during the repeated cycling to 10% elongation. For the subsequent cycling between 0/20% elongation, the same trend remains, with the PU-LEC outperforming the PU-free LEC in both the stretched and relaxed states.

Finally, Fig. 3(d) presents the temporal evolution of the current density and the luminance of a pristine PU-LEC during electrical driving by 40 V, with the first 100 s of operation in the relaxed state, and with a 30% stretching step effectuated thereafter. The luminance and the current density increased with time during the initial operation in the non-stretched state, which provides support for that the ions can redistribute and form electric double layers and electrochemical doping even with PU in the active material. When the device was stretched to 30% elongation (after 100 s), the current density and luminance immediately decreased by over 50%, but thereafter partially recovered in a synchronous manner resulting in a comparable current efficacy before and during stretching. The luminance reached its maximum after approximately 40 s in stretched state, with 65% of the peak luminance in the non-stretched state being retained during stretching. The operational lifetime (here, defined as the time it took for the luminance to drop to half of its peak value) under 30% lateral elongation was 10 min. Importantly, the inset photograph in Fig. 3(d) of the electrically driven PU-LEC at 30% elongation demonstrates that the light emission is highly uniform, despite the device being exposed to extensive stretching.

Conclusions

The emergence of an electroluminescent technology that is intrinsically stretchable, lightweight and low-cost is projected to enable a wide range of novel and functional applications in, for instance, wearables. Herein, we design and systematically develop an intrinsically stretchable LEC, consisting of a PEDOT:PSS/AgNW bilayer cathode and a transparent PEDOT:PSS anode, which sandwich an active material, comprising a hydrophobic blend of a high-molecular-weight conjugated polymer, an ionic liquid and a polymeric PU mechanical stabilizer. We show that this entire device can be fabricated by ambient-air spray-coating, and that it can deliver uniform light emission when stretched to an elongation of 30%. This demonstration is notable in the context of that ambient-air spray-coating can be extremely low cost in comparison to incumbent vacuum-based technologies, and since the developed LEC in addition to being stretchable also is thin and lightweight. Thus, our study represents a first step towards a practical low-cost fabrication of intrinsically stretchable light-emitting devices, which hopefully can find widespread adoption in emerging stretchable and wearable electronics.

Data availability

All experimental data are available for download at: DOI: https://doi.org/10.6084/m9.figshare.29298161.

Conflicts of interest

The authors declare no conflict of interest.

Acknowledgements

The authors are grateful to Tsuyoshi Takeda at Panasonic for generously providing the Beyolex stretchable substrate and to Dr rer. nat. Tilmar Kümmell for support with the SEM measurements. The authors also acknowledge financial support from German Research Foundation (Deutsche Forschungsgemeinschaft (DFG), project ID 498131727), University of Applied Sciences Niederrhein funding program "International exchange of research scientists", the Swedish Research Council (2019-02345), and the Wallenberg Initiative Materials Science for Sustainability (WISE) funded by the Knut and Alice Wallenberg Foundation (WISE-AP01-D02). A. K. acknowledges funding from the European Union (HORIZON MSCA 2023 PF, acronym UNID, grant number 101150699). L. E. acknowledges financial support from the European Union through an ERC Advanced Grant (ERC, InnovaLEC, 101096650).

References

1 S. Zhang, A. Chhetry, Md. A. Zahed, S. Sharma, C. Park, S. Yoon and J. Y. Park, *npj Flexible Electron.*, 2022, **6**, 11.
2 T. Yokota, P. Zalar, M. Kaltenbrunner, H. Jinno, N. Matsuhisa, H. Kitanosako, Y. Tachibana, W. Yukita, M. Koizumi and T. Someya, *Sci. Adv.*, 2016, **2**, e1501856.
3 A. K. Yetisen, J. L. Martinez-Hurtado, B. Ünal, A. Khademhosseini and H. Butt, *Adv. Mater.*, 2018, **30**, 1706910.
4 J. Shen, C. Chui and X. Tao, *Biomed. Opt. Express*, 2013, **4**, 2925.
5 M. K. Smith and K. A. Mirica, *J. Am. Chem. Soc.*, 2017, **139**, 16759–16767.
6 A. Claypole, J. Claypole, J. Leeder, G. Stevens, F. Johnson, N. Bezodis, M. Parker, T. Claypole, D. Gethin and L. Kilduff, *J. Coat. Technol. Res.*, 2023, **20**, 261–273.
7 T. Ray, J. Choi, J. Reeder, S. P. Lee, A. J. Aranyosi, R. Ghaffari and J. A. Rogers, *Curr. Opin. Biomed. Eng.*, 2019, **9**, 47–56.
8 S. Koo and Y. Chae, in *Leading Edge Technologies in Fashion Innovation: Product Design and Development Process from Materials to the End Products to Consumers*, ed. Y.-A. Lee, Springer International Publishing, Cham, 2022, pp. 35–57.
9 Y. Sun, W. M. Choi, H. Jiang, Y. Y. Huang and J. A. Rogers, *Nat. Nanotechnol.*, 2006, **1**, 201–207.
10 D. J. Lipomi, B. C.-K. Tee, M. Vosgueritchian and Z. Bao, *Adv. Mater.*, 2011, **23**, 1771–1775.
11 W. Weng, Q. Sun, Y. Zhang, S. He, Q. Wu, J. Deng, X. Fang, G. Guan, J. Ren and H. Peng, *Adv. Mater.*, 2015, **27**, 1363–1369.
12 D. Yin, J. Feng, R. Ma, Y.-F. Liu, Y.-L. Zhang, X.-L. Zhang, Y.-G. Bi, Q.-D. Chen and H.-B. Sun, *Nat. Commun.*, 2016, **7**, 11573.
13 D. Yin, N.-R. Jiang, Y.-F. Liu, X.-L. Zhang, A.-W. Li, J. Feng and H.-B. Sun, *Light: Sci. Appl.*, 2018, **7**, 35.
14 T. Kim, H. Lee, W. Jo, T. Kim and S. Yoo, *Adv. Mater. Technol.*, 2020, **5**, 2000494.
15 F. Suarez, D. P. Parekh, C. Ladd, D. Vashaee, M. D. Dickey and M. C. Öztürk, *Appl. Energy*, 2017, **202**, 736–745.
16 M. D. Dickey, *Adv. Mater.*, 2017, **29**, 1606425.
17 Y. Zhang, S. Xu, H. Fu, J. Lee, J. Su, K.-C. Hwang, J. A. Rogers and Y. Huang, *Soft Matter*, 2013, **9**, 8062.
18 R.-H. Kim, D.-H. Kim, J. Xiao, B. H. Kim, S.-I. Park, B. Panilaitis, R. Ghaffari, J. Yao, M. Li, Z. Liu, V. Malyarchuk, D. G. Kim, A.-P. Le, R. G. Nuzzo, D. L. Kaplan, F. G. Omenetto, Y. Huang, Z. Kang and J. A. Rogers, *Nat. Mater.*, 2010, **9**, 929–937.
19 S. Ji, B. G. Hyun, K. Kim, S. Y. Lee, S.-H. Kim, J.-Y. Kim, M. H. Song and J.-U. Park, *NPG Asia Mater.*, 2016, **8**, e299.
20 M. Nogi, N. Komoda, K. Otsuka and K. Suganuma, *Nanoscale*, 2013, **5**, 4395.
21 T. Kim, J. S. Price, A. Grede, S. Lee, G. Choi, W. Guan, T. N. Jackson and N. C. Giebink, *Adv. Mater. Technol.*, 2018, **3**, 1800067.
22 B. Jang, S. Won, J. Kim, J. Kim, M. Oh, H. Lee and J. Kim, *Adv. Funct. Mater.*, 2022, **32**, 2113299.
23 J. H. Koo, D. C. Kim, H. J. Shim, T. Kim and D. Kim, *Adv. Funct. Mater.*, 2018, **28**, 1801834.
24 J. Yoo, S. Li, D.-H. Kim, J. Yang and M. K. Choi, *Nanoscale Horiz.*, 2022, **7**, 801–821.
25 J. Liu, J. Wang, Z. Zhang, F. Molina-Lopez, G.-J. N. Wang, B. C. Schroeder, X. Yan, Y. Zeng, O. Zhao, H. Tran, T. Lei, Y. Lu, Y.-X. Wang, J. B.-H. Tok, R. Dauskardt, J. W. Chung, Y. Yun and Z. Bao, *Nat. Commun.*, 2020, **11**, 3362.
26 H. Zhou, S. J. Han, A. K. Harit, D. H. Kim, D. Y. Kim, Y. S. Choi, H. Kwon, K. Kim, G. Go, H. J. Yun, B. H. Hong, M. C. Suh, S. Y. Ryu, H. Y. Woo and T. Lee, *Adv. Mater.*, 2022, **34**, 2203040.
27 Y. Go, H. Park, Y. Zhu, K. Yoo, J. Kwak, S. Jin and J. Yoon, *Adv. Funct. Mater.*, 2023, **33**, 2215193.
28 K. Schlingman, Y. Chen, R. S. Carmichael and T. B. Carmichael, *Adv. Mater.*, 2021, **33**, 2006863.
29 J.-H. Kim and J.-W. Park, *Sci. Adv.*, 2021, **7**, eabd9715.
30 Z. Zhang, W. Wang, Y. Jiang, Y.-X. Wang, Y. Wu, J.-C. Lai, S. Niu, C. Xu, C.-C. Shih, C. Wang, H. Yan, L. Galuska, N. Prine, H.-C. Wu, D. Zhong, G. Chen, N. Matsuhisa, Y. Zheng, Z. Yu, Y. Wang, R. Dauskardt, X. Gu, J. B.-H. Tok and Z. Bao, *Nature*, 2022, **603**, 624–630.
31 S. G. R. Bade, X. Shan, P. T. Hoang, J. Li, T. Geske, L. Cai, Q. Pei, C. Wang and Z. Yu, *Adv. Mater.*, 2017, **29**, 1607053.
32 Q. Pei, G. Yu, C. Zhang, Y. Yang and A. J. Heeger, *Science*, 1995, **269**, 1086–1088.
33 J.-K. Lee, D. S. Yoo, E. S. Handy and M. F. Rubner, *Appl. Phys. Lett.*, 1996, **69**, 1686–1688.
34 J. E. Namanga, N. Gerlitzki and A. Mudring, *Adv. Funct. Mater.*, 2017, **27**, 1605588.
35 L. Mardegan, C. Dreessen, M. Sessolo, D. Tordera and H. J. Bolink, *Adv. Funct. Mater.*, 2021, **31**, 2104249.
36 M. H. Bowler, T. Guo, L. D. Bastatas, M. D. Moore, A. V. Malko and J. D. Slinker, *Mater. Horiz.*, 2017, **4**, 657–664.
37 S. Uchida and Y. Nishikitani, *Adv. Funct. Mater.*, 2020, **30**, 1907309.
38 S. Tang, P. Lundberg, Y. Tsuchiya, J. Ràfols-Ribé, Y. Liu, J. Wang, C. Adachi and L. Edman, *Adv. Funct. Mater.*, 2022, **32**, 2205967.
39 S. van Reenen, P. Matyba, A. Dzwilewski, R. A. J. Janssen, L. Edman and M. Kemerink, *J. Am. Chem. Soc.*, 2010, **132**, 13776–13781.

40 A. Sandström, H. F. Dam, F. C. Krebs and L. Edman, *Nat. Commun.*, 2012, **3**, 1002.
41 A. Asadpoordarvish, A. Sandström, C. Larsen, R. Bollström, M. Toivakka, R. Österbacka and L. Edman, *Adv. Funct. Mater.*, 2015, **25**, 3238–3245.
42 G. Hernandez-Sosa, S. Tekoglu, S. Stolz, R. Eckstein, C. Teusch, J. Trapp, U. Lemmer, M. Hamburger and N. Mechau, *Adv. Mater.*, 2014, **26**, 3235–3240.
43 J. Liang, L. Li, X. Niu, Z. Yu and Q. Pei, *J. Phys. Chem. C*, 2013, **117**, 16632–16639.
44 E. Auroux, G. Huseynova, J. Ràfols-Ribé, V. Miranda La Hera and L. Edman, *RSC Adv.*, 2023, **13**, 16943–16951.
45 J. Zimmermann, L. Porcarelli, T. Rödlmeier, A. Sanchez-Sanchez, D. Mecerreyes and G. Hernandez-Sosa, *Adv. Funct. Mater.*, 2018, **28**, 1705795.
46 Z. Yu, L. Hu, Z. Liu, M. Sun, M. Wang, G. Grüner and Q. Pei, *Appl. Phys. Lett.*, 2009, **95**, 203304.
47 Z. Yu, X. Niu, Z. Liu and Q. Pei, *Adv. Mater.*, 2011, **23**, 3989–3994.
48 H. L. Filiatrault, G. C. Porteous, R. S. Carmichael, G. J. E. Davidson and T. B. Carmichael, *Adv. Mater.*, 2012, **24**, 2673–2678.
49 J. Liang, L. Li, X. Niu, Z. Yu and Q. Pei, *Nat. Photonics*, 2013, **7**, 817–824.
50 S. J. Han, H. Zhou, H. Kwon, S. Woo and T. Lee, *Adv. Funct. Mater.*, 2023, **33**, 2211150.
51 A. Sandström, A. Asadpoordarvish, J. Enevold and L. Edman, *Adv. Mater.*, 2014, **26**, 4975–4980.
52 M. Vosgueritchian, D. J. Lipomi and Z. Bao, *Adv. Funct. Mater.*, 2012, **22**, 421–428.
53 J.-Y. Lee, S. T. Connor, Y. Cui and P. Peumans, *Nano Lett.*, 2008, **8**, 689–692.
54 I. Verboven, J. Silvano, K. Elen, H. Pellaers, B. Ruttens, J. D'Haen, M. K. Van Bael, A. Hardy and W. Deferme, *Adv. Eng. Mater.*, 2022, **24**, 2100808.
55 J. Xu, A. Sandström, E. M. Lindh, W. Yang, S. Tang and L. Edman, *ACS Appl. Mater. Interfaces*, 2018, **10**, 33380–33389.
56 G. Y. Margulis, M. G. Christoforo, D. Lam, Z. M. Beiley, A. R. Bowring, C. D. Bailie, A. Salleo and M. D. McGehee, *Adv. Energy Mater.*, 2013, **3**, 1657–1663.
57 A. Das and P. Mahanwar, *Adv. Ind. Eng. Polym. Res.*, 2020, **3**, 93–101.
58 A. Mishra, V. K. Aswal and P. Maiti, *J. Phys. Chem. B*, 2010, **114**, 5292–5300.

